Applied Physics A (2021) 127:71
https://doi.org/10.1007/s00339-020-04227-5

Applied Physics A
Materials Science & Processing

Silver nanoparticles in natural zeolites incorporated into commercial coating: antibacterial study

E. I. Torres-Flores[1] · N. S. Flores-López[2] · C. E. Martínez-Núñez[3] · J. C. Tánori-Córdova[1] · M. Flores-Acosta[3] · M. Cortez-Valadez[4]

Received: 3 September 2020 / Accepted: 17 December 2020 / Published online: 4 January 2021

Abstract

In this study, silver nanoparticles on chabazite, clinoptilolite, and clinoptilolite-stilbite natural zeolites were synthesized. The nanomaterials were incorporated into commercial coatings and afterward, the antibacterial activity was carried out. The zeolites were exposed to the activation step before the ion-exchange process with the precursor. The optical properties of the nanoparticles were studied through UV–Vis and FT-IR spectroscopy. Morphological and structural parameters were analyzed through TEM microscopy. The particle size of about 2–20 nm with spherical approach morphologies was obtained. Using XPS spectroscopy, the silver oxidation state was determined. The obtained nanomaterials showed antibacterial activity after their incorporation into the coatings. For this analysis, the Kirby-Bauer method was performed, studying the material against *E. coli* ATCC 25,922, *K. pneumoniae* ATCC 25,955, and *K. pneumoniae* ESBL + bacteria.

Keywords Natural zeolites · Antibacterial effect · Silver nanoparticles · Antibacterial coatings

1 Introduction

The nanostructured systems have modified the functional perspective of materials used in different domains of application. This has improved biosensors such as biomarkers, drug delivery, and theranostics applications [1–5]. The zeolites have been used as templates or mediums to synthesize nanoparticles. These have grown considerably in the last few years, increasing their use in the application of nanomaterials, and providing them greater stability [6]. The ion-exchange capacity means that these aluminosilicates are highly attractive for the synthesis and stabilization of nanostructured and sub-nanostructured materials [7]. In such templates, several structures with different applications and morphologies have been obtained, such as nanowires, nanostars, hollow nanospheres, and ultra-small clusters [8–11]. The use of natural zeolites to obtain nanostructures has been increasing in recent years. Among these are chabazite, clinoptilolite, heulandite, mordenite, etc. [12–15]. As some types of zeolites have antibacterial properties, this usually represents a great synergy with nanostructured materials, enhancing such applications [16].

The synthetic zeolites in relation to natural zeolites are most used for nanoparticles obtaining. Using natural zeolites promotes the sustainable utilization of natural resources. The chabazite, clinoptilolite, and clinoptilolite-stilbite zeolites have been selected since these are natural zeolites obtained from regional deposits. With the results achieved in this work, we intend to enhance its application. Concerning other types of zeolite, those indicated in this work symbolize a representatively lower cost.

Supplementary Information The online version contains supplementary material available at https://doi.org/10.1007/s00339-020-04227-5.

✉ M. Cortez-Valadez
manuelcortez@live.com; jose.cortez@unison.mx

[1] Depto. de Investigación en Polímeros y Materiales, Universidad de Sonora, Blvd. Encinas y Rosales s/n, 83000 Hermosillo, Sonora, Mexico

[2] Centro de Física Aplicada y Tecnología Avanzada (CFATA), Universidad Nacional Autónoma de México (UNAM), Blvd. Juriquilla 3000, Querétaro, Mexico

[3] Departamento de Investigación en Física, Universidad de Sonora, Apdo. Postal 5-88, 83190 Hermosillo, Sonora, Mexico

[4] CONACYT-Departamento de Investigación en Física, Universidad de Sonora, Apdo. Postal 5-88, 83190 Hermosillo, Sonora, Mexico

Additionally, it has been reported that Ag NPs are obtained in a zeolite matrix such as the mordenite, 4A, and ZSM-5, with spherical geometry, regularly [17–19]. In some cases, the antibacterial capacity of Ag NPs in the zeolite matrix has been analyzed [20, 21]. On the other hand, metallic nanoparticles exhibit the optical property known as the surface plasmon resonance (SPR) easily tunable and directly dependent on the morphological and dimensional parameters [22]. This property has been related to the antibacterial properties, allowing the identification of structural parameters that increase the antimicrobial effect [23]. Due to this, metallic nanoparticles obtaining especially silver, in a template that previously exhibited an antibacterial effect, enhances its properties [24]. Additionally, up-conversion nanoparticles (UCNPs) and carbon dots have provided applications in cancer therapy [25, 26]. Zeolite-stabilized nanoparticles can be a suitable medium for immersion in other coating types, preserving the antibacterial properties of the nanoparticles. In the case of clinoptilolite-stilbite and heulandite, the application, deposition, and subsequent characterization studies in coatings have not been entirely addressed [27]. There are nanostructured materials incorporated in coatings that achieve an acceptable antibacterial effect [28]. However, usually the methodology for their incorporation requires the use of sophisticated equipment and time-consuming synthesis processes.

Recently, Duangkamon Jiraroj et al. have evaluated the bactericidal activity in coatings with Ag^+ ions and Ag NP, achieving the optimal combination of these to enhance the above applications using synthetic zeolite A [29]. The bactericide efficiency of zeolite coatings with silver nanoparticles has been evaluated by Mpenyana-Monyatsi et al. removing bacteria from groundwater using low concentrations and reaching 100% efficiency [30]. Galeano et al. obtained a coating based on paint zinc incorporated nanoparticles for application on steel surfaces. Achieving a bactericidal effect on Bacillus anthracis, B. cereus, and B. subtilis bacteria. In the previously mentioned cases, the study focuses only on standardized bacterial strains [31].

The present investigation addresses the comparative study of stabilized nanoparticles in chabazite, clinoptilolite, and clinoptilolite-stilbite natural zeolites including both standardized and extended-spectrum β-lactamases-positive (ESBL+) bacterial cultures. We consider the analysis of its antibacterial property after the incorporation in commercial coatings. Additionally, the proposed method represents an agreement with the green chemistry philosophy and means an extremely low cost for nanomaterials application.

2 Materials and methods

2.1 Ag NPs synthesis and incorporation into coatings

Three types of natural zeolite were used as a matrix (chabazite, clinoptilolite-stilbite, and clinoptilolite) for hosting the Ag NPs. The activation and cleaning process of the zeolite was carried out as reported by J. F. Román. [32] The Ag NPs synthesis was carried out employing the ion-exchange property of the zeolites and based on the method previously proposed by M. Flores and coworkers [33–35]. A detailed description of this process has been included in the Supplemental information.

For the coatings, we use the classic white commercial paint from the *Osel* company. A portion of zeolite-Ag NPs of 0.25 g was combined with 20 ml of paint. The mixture was magnetically stirred for 20 min. Using the dip-coating method a glass slide was employed as a substrate. This was kept at 5 s immersion time and it was dried at room temperature for 24 h. Subsequently, the coated glass slides were sectioned to 1 cm^2 to carry out the antibacterial study. This procedure was done for all zeolite types, as shown in scheme 1.

2.2 Antibacterial study

The following cultures were used for the antibacterial tests: *Escherichia coli* ATCC 25,922, *Klebsiella pneumoniae* ATCC 25,955, and *Klebsiella pneumoniae* ESBL+.

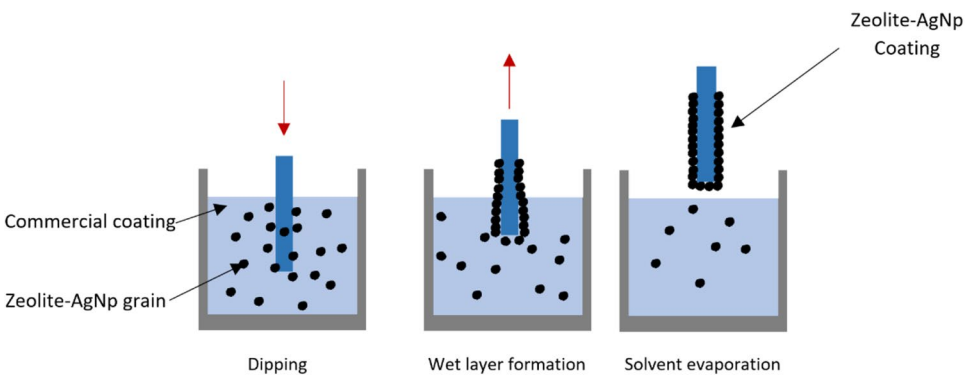

Scheme 1 Process of slide coating with zeolite-Ag NP

These were developed in culture media: tryptic soy broth and agar for standard methods.

For the inhibition halo measurement by the Kirby-Bauer method, a bacterial inoculum was performed to match the 0.5 (1.5×10^8 UFC/ml) McFarland standard. This was massively seeded on a plate with culture medium, then 1 cm^2 glass sections with coating were placed. It was incubated for 24 h at 37 °C, then the inhibition halo was measured.

3 Results and discussion

The low-resolution XPS spectra are included in Fig. 1 and were obtained using a Mg source. These spectra correspond to clinoptilolite-stilbite, clinoptilolite, and chabazite, Fig. 1a–c, respectively. In all cases the high-resolution spectrum on the silver region is shown in the inset. The signals associated with oxygen, silicon, and aluminum, which represent the framework of the zeolite, are observed. In the low-resolution XPS spectrum, it is also possible to observe Auger transitions are located at 990, 902, and 745 eV

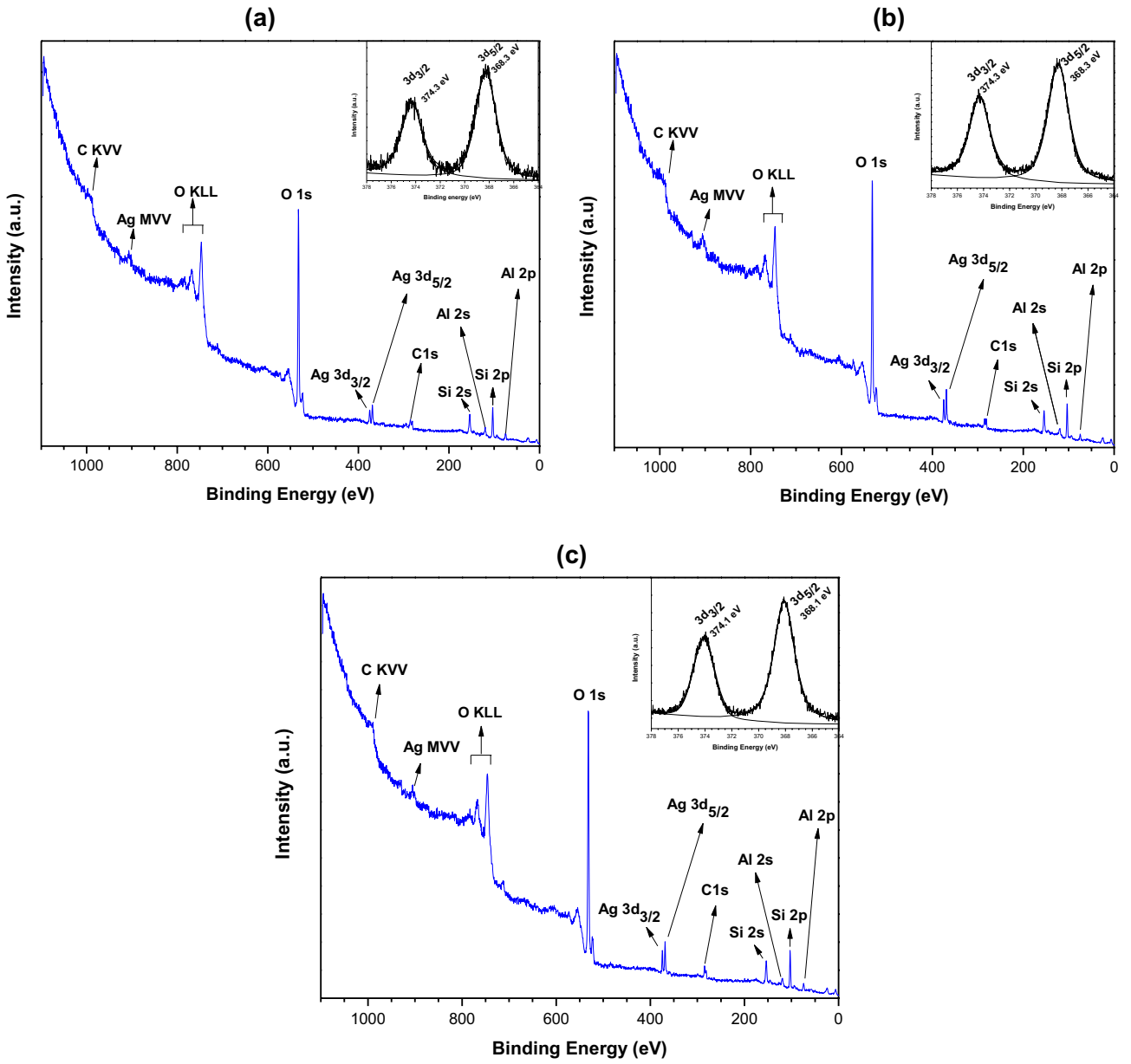

Fig. 1 Low-resolution XPS spectra and high-resolution spectrum at 3d silver region (inset): **a** clinoptilolite-stilbite, **b** clinoptilolite, and **c** chabazite

approximately. Which, according to Moulder et al., can be associated with Carbon (KVV), Silver (MVV), and Oxygen (KLL) [36].

Similarly, it is possible to observe the carbon 1 s signal. Analyzing the high-resolution spectrum in the 364–378 eV region, it is observed that this adjustment closely presents a good match to the signal obtained experimentally. Here, two signals with peaks at 374.3 eV and 368.3 eV with an energy difference between them of 6 eV, corresponding to the $3d_{3/2}$ (374.3 eV) and $3d_{5/2}$ (368.3 eV) associated to silver [36–38].

Figure 2 displays the optical absorption spectra, corresponding to Ag NPs stabilized in the different zeolite types. For all cases, a molarity of 0.07 M of $AgNO_3$ was considered. The experimental signal is produced by the contribution of 4 bands, located at 206, 282, 364, and 496 nm for the case of clinoptilolite-stilbite (Fig. 2a). For clinoptilolite (Fig. 2b), these bands are located at 200, 259, 362, and 516 nm, and for chabazite (Fig. 2c) at 203, 277, 474, and 625 nm. Figure 2d provides a comparison of Ag NPs optical absorption in the three zeolites types. The absorption bands in the range of 200–259 nm have been associated with the presence of silver ions by other systems. [39] However, in some reports there are associated bands between 277 and 282 nm to the presence of Ag_{147} clusters with cube-octahedral morphology. [40] The SPR in Ag NPs with spherical type geometry is regularly observed between 400 and 530 nm. [41] The absorption bands obtained between the region of 496–516 in Fig. 2 represent such a case.

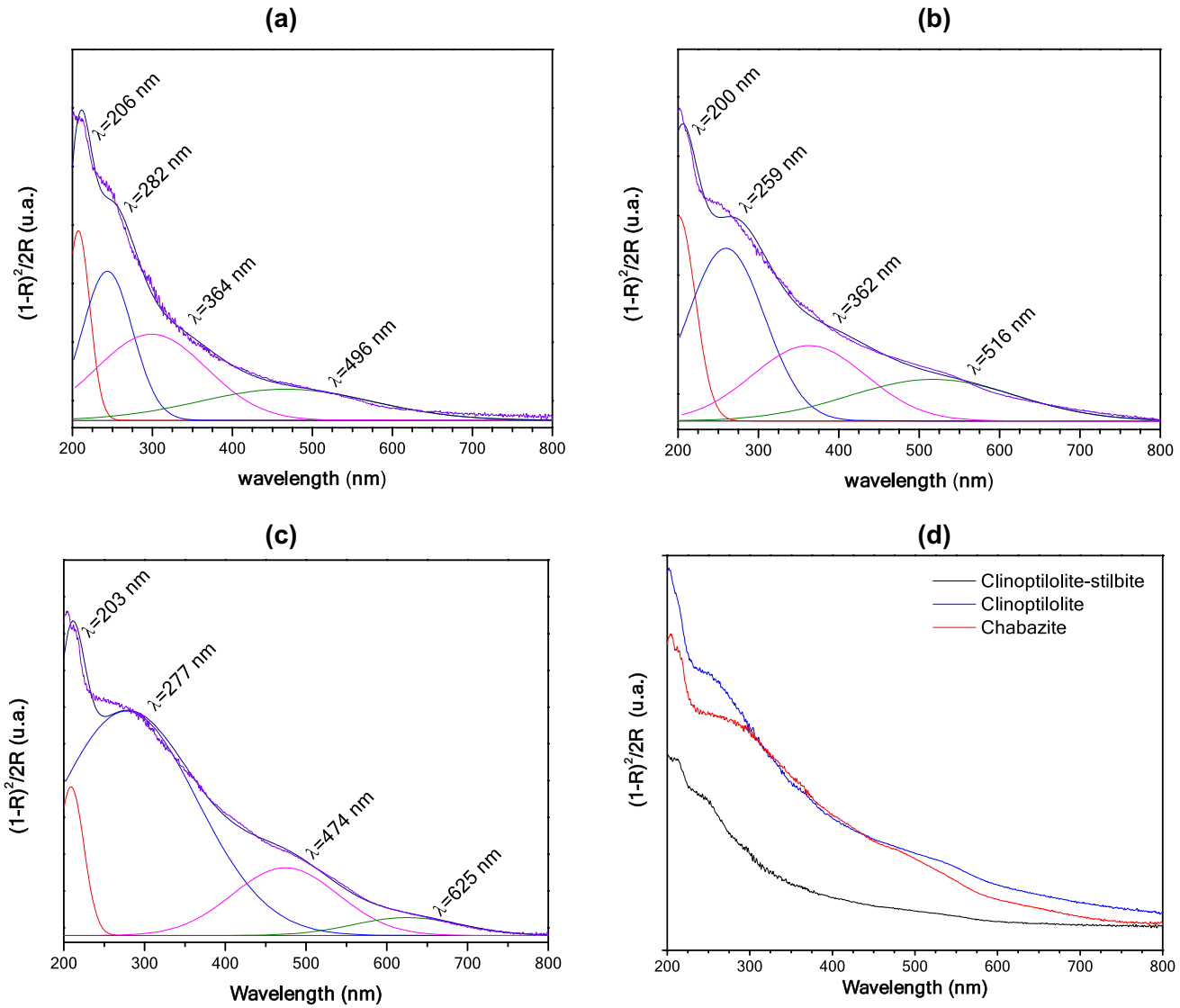

Fig. 2 Optical absorption of Ag NPs and deconvolutions in **a** clinoptilolite-stilbite, **b** clinoptilolite, **c** chabazite, and **d** absorption spectra of the three types of zeolite hosting Ag NPs

In other templates, nanoparticles with triangular geometries, plates, and cubes have been obtained. These have exhibited SPR in near red regions [42, 43].

In addition, Fig. 2d shows that the absorption maxima (SPR) have slight shifts. This suggests that different types of zeolite can influence on particle size, even considering the same parameters of the synthesis method. With a particular feature for different types of applications [34, 38, 44–46].

On the other hand, the (black line) in Fig. 3 indicates the result of activated zeolite types and the b (red line) indicates the result of zeolite with Ag NP (0.07 M). In the spectra, absorption peaks are observed around 3300 and 1630 cm^{-1}, these are associated to water molecules interacting with Na^{+} and Ca^{+} at the channels and cages of the zeolite skeletal structure [47]. In the vibrational spectrum regions, it is possible to observe behaviors or modifications associated with the trend of metallic species to form aqua-complexes and hydration in aqueous media [48]. Featuring slight alterations in bands located on the 3700–3100 range cm^{-1} (OH^{-} groups present in the zeolite structure). As well as regions from 800 to 500 cm^{-1} affected by metal cations sorption. In this work, for the varieties of zeolite involved, slight modifications are observed on these vibrational regions. However, for clinoptilolite zeolite, a stronger modification is observed on the 3700–3100 cm^{-1} and 800–500 cm^{-1} region. Meaning that it is a representation of the silver species [48]. Other bands emerge around 1020, 770, 535, and 458 cm^{-1}. The band in 1020 cm^{-1} corresponds to vibration modes of

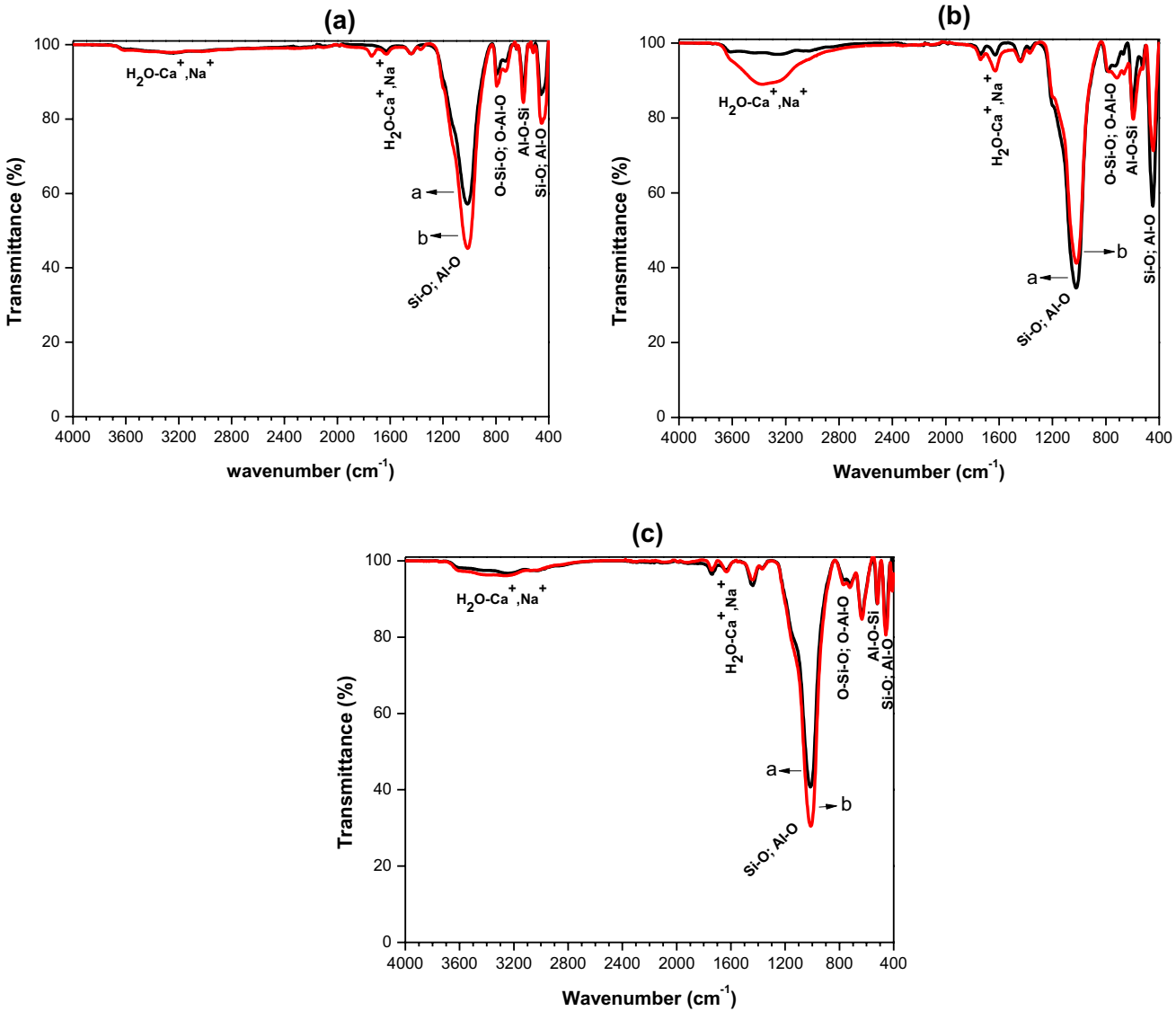

Fig. 3 FT-IR spectra of individual activated zeolite types (black line) and hosting Ag NPs (red line): **a** Clinoptilolite-Stilbite, **b** Clinoptilolite, and **c** Chabazite

asymmetric stretching of Si–O and Al–O bonds [49]. The band at 770 cm^{-1} is assigned to stretching vibration modes of the O–Si–O and O–Al–O groups. Whereas the band found in 535 cm^{-1} is assigned to the torsional vibrations of the Al–O–Si bonds. [50] Finally, the 458 cm^{-1} band is associated with the bending vibrations of the Si–O and Al-O bonds [51–53].

The morphology and structural parameters of the nanoparticles were obtained by TEM (Fig. 4). Figure 4a shows the micrographs for the nanoparticles synthesized using clinoptilolite-stilbite. The interplanar distance (inset) is 1.45 Å, which can be associated with the plane (1 1 0) [54]. The particle size histogram in Fig. 4b represents the distribution of the particles in Fig. 4a. It is observed that the size range is between 2 and 13 nm, with two prominent populations of 5 and 8 nm. Moreover, using the Clinoptilolite as a template, a decrease in the particle size has been obtained (Fig. 4c). In this matrix, the predominant size is between 4 and 6 nm. Likewise, the interplanar distance found is associated with the plane (1 1 0) corresponding to the hexagonal silver space group P63/mmc. Although the size range is wider, it is limited by parameters of 2–20 nm as shown in Fig. 4d. In the Chabazite study, as in the previous cases, nanoparticles with spherical morphologies were obtained as shown in Fig. 4e. However, the size range has a better delimitation between 3 and 8.5 nm. Similarly, the predominant nanoparticle population is located between 4.5 and 5 nm as shown in Fig. 4f. Once again, the (1 1 0) plane was identified.

Using the three zeolite types with the same parameters of the proposed synthesis method, slight shifts in the size range of the nanoparticles have been obtained. This behavior may depend on the size of the zeolite crystal and sometimes on the silicon/aluminum ratio [55, 56]. In other zeolite species, particles with sizes ranging from 50 nm have been obtained [57]. Since the predominant size of the nanoparticles obtained in this work is less than 30 nm, it is attractive for drug delivery applications. Because they can be easily removed from the bloodstream [58]. Nanoparticles with well-defined regions of size have promoted their application for theragnostic purposes [59].

In addition, theoretical studies using DFT, Monte Carlo simulation, molecular dynamics, etc., have indicated that small clusters (below 1 nm) are confined to the zeolite channels and exhibit interaction with oxygen atoms within 2.88 ± 0.02 Å [60]. Sub-nanometric particles confined to the zeolite structure represent an application field on catalysis, achieving selective characteristics in specific reactions [61].

Table 1 shows the elemental analysis by EDS for zeolites with Ag NPs. The amount of oxygen, aluminum, and silicon is higher than the amount of potassium, iron, magnesium, calcium, sulfur, and silver. Since these elements constitute the skeletal structure of the zeolite. Additionally, it is observed that the amount of silver after treatment was variable according to the zeolite type. In this case, the clinoptilolite-stilbite achieved the highest amount of silver with 14.43 wt%, compared to 4.21 wt% and 3.90 wt% obtained for clinoptilolite and chabazite, respectively.

For the inhibition halo study by the Kirby-Bauer method, the control cultures were tested with a 10 µg Gentamicin disk used as positive control. Whereas an activated zeolite coating and a zeolite coating from deposit were used as a negative control.

Figure 5 provides a schematic representation of the results obtained. The horizontal axis represents the Ag NPs zeolite samples obtained from 0.07 M $AgNO_3$ aqueous solutions and the corresponding controls. On the vertical axis, the inhibition halo measurement is presented in millimeter (mm) units. As observed in the case of Chabazite-Ag NPs, for *E. Coli* a higher inhibition was shown with a diameter of 17 mm, better than the 15 mm obtained by Clinoptilolite-stilbite and Clinoptilolite. The zeolites extracted from the deposit, as well as the ones activated later, provided a better antibacterial effect than the positive control. In the case of *K. pneumoniae* ATCC, the antibacterial effect of zeolites by incorporating nanoparticles did not increase significantly. With the clinoptilolite-stilbite, it was possible to increase the inhibition radius by only 1 mm. In other cases, the radius was increased up to 2 mm.

Additionally, against *K. pneumoniae ESBL* + bacteria, clinoptilolite showed an enhanced inhibition radius of up to 19 mm. Other authors have reported Ag NPs stabilized in zeolite ZSM-5 against *E. coli* and *P. aeruginosa*, reaching inhibition radii up to 10 mm [62]. As zeolites are powders and have micro-pores, their application in coatings is attractive. The results reported in this work suggest that using only these types of natural zeolite in combination with commercial paint, a superior antibacterial effect to the positive control is obtained. This combined antibacterial effect, between zeolites and Ag NPs, is not commonly associated between the stabilizer and the precursor [63]. This behavior has been observed in some plant extracts when these are used as reducing agents/stabilizers of metallic nanoparticles [64].

In general, in this work the Ag NPs supported in chabazite, obtained a prominent antibacterial activity against the studied cultures. According to TEM analysis, chabazite-hosted Ag NPs have the smallest nanoparticle size distribution (3—8.5 nm), which is a factor that contributes to antibacterial capacity [65]. According to the EDS analysis, this behavior could be due to the chabazite contain a lower amount of silver (3.90 wt%).

The most susceptible bacteria to Ag NPs were *Escherichia coli*, although the *K. pneumoniae ESBL* + variant showed slightly higher resistance to Ag NPs. This can be attributed to the fact that bacteria of this genre possess a protective polysaccharide capsule [66].

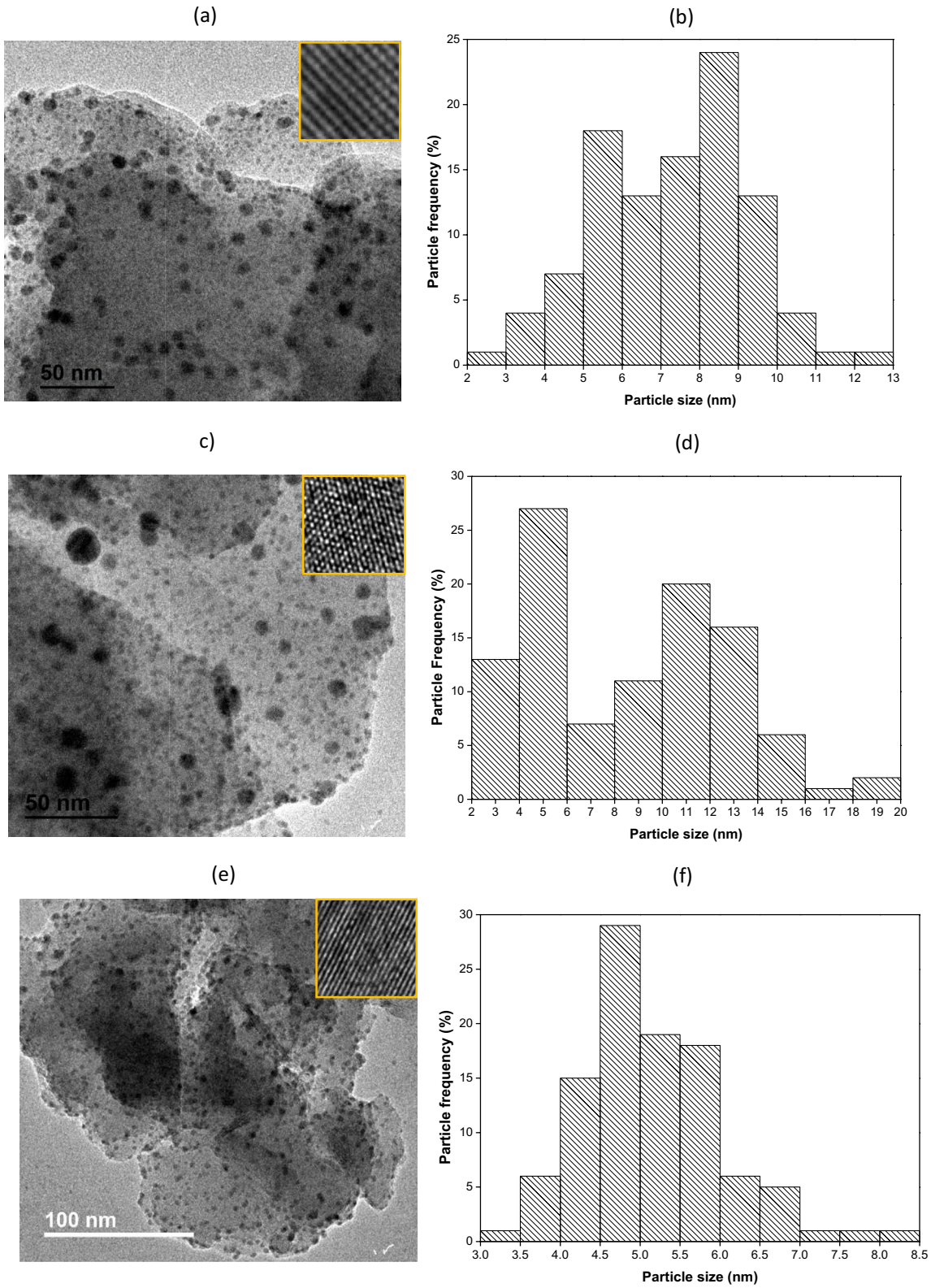

Fig. 4 TEM images of Ag NPs, interplanar distance (inset) and related particle size histogram: **a** Clinoptilolite-Stilbite, **b** Clinoptilolite, and **c** Chabazite

Table 1 Elemental analysis for zeolite types with Ag NPs

Element	Clinoptilolite-stilbite (%)	Clinoptilolite (%)	Chabazite (%)
Oxygen	39.10	42.50	42.08
Aluminum	9.08	8.28	11.29
Silicon	33.96	42.70	40.33
Potassium	*	1.02	*
Iron	0.47	0.53	1.28
Magnesium	0.82	0.25	0.72
Calcium	1.14	0.52	*
Sulfur	1.00	*	0.40
Silver	14.43	4.21	3.90

*Excluded from the sample

4 Conclusions

From this study, it is confirmed that a material with antibacterial properties based on Ag NPs and natural zeolites was obtained. The Zeolite- Ag NPs systems exhibited features to be incorporated into commercial paint and still retain their antibacterial properties. The use of different zeolite types is indicated without a rigorous cleaning process. In the zeolite types, the surface plasmon resonance located in the UV–Vis region was observed in a different position than the silver bulk absorption bands.

In the test of the antibacterial activity after the incorporation of the nanoparticles in commercial coatings, the effect of

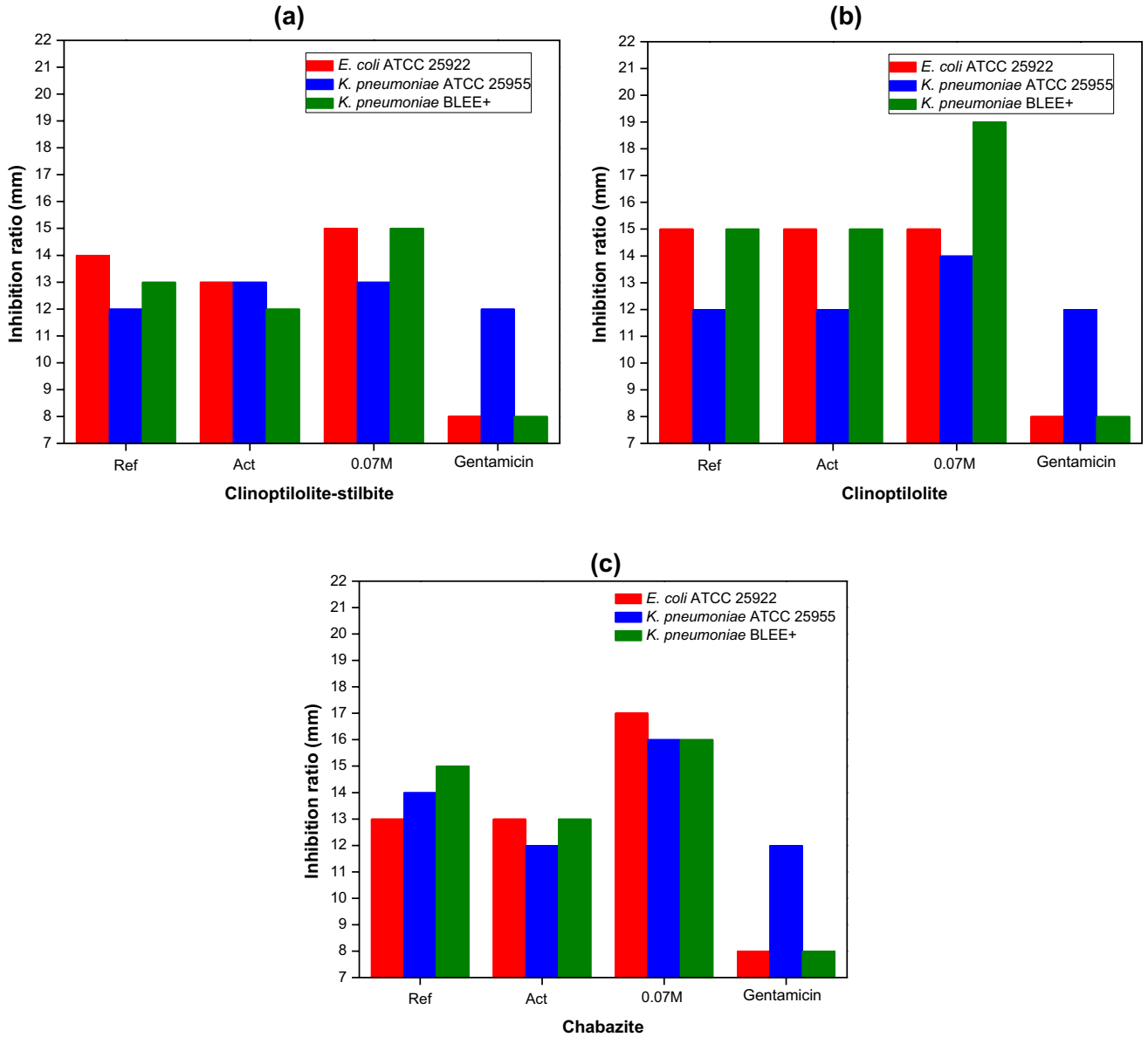

Fig. 5 Inhibition radius (mm) given by the gentamicin, zeolite, zeolite-Ag NP systems by the Kirby-Bauer method. **a** Clinoptilolite-stilbite, **b** Clinoptilolite and **c** Chabazite

the material on the cultures *Escherichia coli, Klebsiella pneumoniae ATCC* 25,955, and *Klebsiella pneumoniae ESBL+* was confirmed. A higher inhibition halo was observed compared to the positive control used. The nanoparticles obtained in the Chabazite were smaller in size, between 2 and 8.5 nm. These presented prominent antibacterial activity. Clinoptilolite-stilbite was able to host higher amounts of silver, achieving a quantity of 14.43 wt%. In all cases, the nanoparticles were smaller than 20 nm.

The results obtained can be generalized and applied on different coatings such as resins, natural oils, sealants, and ceramic paste, to prevent bacterial growth on several surfaces.

Acknowledgements This work was supported by project A1-S-46242 of the CONACYT Basic Science. The author M. Cortez-Valadez appreciates the support by "Cátedras CONACYT" program. Special thanks to the support brought by the Laboratory of Transmission Electron Microscopy at the University of Sonora.

References

1. S. Singh, A.A.S. Gill, M. Nlooto, R. Karpoormath, Prostate cancer biomarkers detection using nanoparticles based electrochemical biosensors. Biosensors Bioelectron **137**, 213–221 (2019)
2. H. Nagar, N. Sahu, V.V. Basava Rao, S. Sridhar, Surface modification of sulfonated polyethersulfone membrane with polyaniline nanoparticles for application in direct methanol fuel cell. Renewable Energy **146**, 1262–1277 (2020)
3. R.M. Pallares, N.T.K. Thanh, X. Su, Sensing of circulating cancer biomarkers with metal nanoparticles. Nanoscale **11**, 22152–22171 (2019)
4. M. Manzano, M. Vallet-Regí, Mesoporous silica nanoparticles for drug delivery. Adv. Funct. Mater. 1902634, (2019)
5. S.M. Dadfara, K. Roemhild, N.I. Drude, S. Stillfried, R. Knüchel, F. Kiessling, T. Lammers, Adv. Drug Delivery Rev. **138**, 302–325 (2019)
6. A.W. Petrov, D. Ferri, O. Kröcher, J.A. van Bokhoven, Design of stable palladium-based zeolite catalysts for complete methane oxidation by postsynthesis zeolite modification. ACS Catal. **9**(3), 2303–2312 (2019)
7. J. Vergara-Figueroa, S. Alejandro-Martín, H. Pesenti, F. Cerda, A. Fernández-Pérez, W. Gacitúa, Obtaining nanoparticles of Chilean natural zeolite and its ion exchange with copper salt (Cu2+) for antibacterial applications. Materials **12**, 2202 (2019)
8. X. Lin, J. Lin, C. Zeng, J. Niu, R. Chenna Krishna Reddy, J. Liu, Y. Cai, Z. Yuan, J. Colloid Interface Sci. **565**, 156–166 (2020)
9. C. Carrillo-Carrión, R. Martínez, M.F. Navarro Poupard, B. Pelaz, E. Polo, A. Arenas-Vivo, A. Olgiati, P. Taboada, M.G. Soliman, Ú. Catalán, S. Fernández-Castillejo, R. Solà, W.J. Parak, P. Horcajada, R.A. Alvarez-Puebla, P. del Pino, Aqueous stable gold nanostar/ZIF-8 nanocomposites for light-triggered release of active cargo inside living cells. Angewandte Chemie Int. Edition **58**, 7078–7082 (2019)
10. K. Wang, M. Dong, J. Li, P. Liu, K. Zhang, J. Wang, W. Fan, Facile fabrication of ZSM-5 zeolite hollow spheres for catalytic conversion of methanol to aromatics. Catal. Sci. Technol. **7**, 560–564 (2017)
11. Q. Sun, N. Wang, Yu. Risheng Bai, T.Z. Hui, D.A. Do, P. Zhang, L. Song, S. Miao, Yu. Jihong, Synergetic effect of ultrasmall metal clusters and zeolites promoting hydrogen generation. Adv. Sci. **6**, 1802350 (2019)
12. M. Moliner, J.E. Gabay, C.E. Kliewer, R.T. Carr, J. Guzman, G.L. Casty, P. Serna, A. Corma, Reversible transformation of Pt nanoparticles into single atoms inside high-silica chabazite zeolite. J. Am. Chem. Soc. **138**, 15743–15750 (2016)
13. H. Derikvandi, A. Nezamzadeh-Ejhieh, A comprehensive study on electrochemical and photocatalytic activity of SnO2-ZnO/clinoptilolite nanoparticles. J. Mol. Catalysis A Chem. **426**(PART A), 158–169 (2017)
14. D. Lin, H. Zhu, Wu. Yining, Lu. Teng, Y. Liu, X. Chen, C. Peng, C. Yang, X. Feng, Morphological insights into the catalytic aquathermolysis of crude oil with an easily prepared high-efficiency Fe3O4-containing catalyst. Fuel **245**, 420–428 (2019)
15. P. Sánchez-López, Y. Kotolevich, S. Miridonov, F. Chávez-Rivas, S. Fuentes, V. Petranovskii, Bimetallic AgFe Systems on Mordenite: effect of cation deposition order in the NO reduction with C3H6/CO. Catalysts **9**, 58 (2019)
16. M. Nasrollahzadeh, T. Baran, N. Yılmaz Baran, M. Sajjadi, M.R. Tahsili, M. Shokouhimehr, Pd nanocatalyst stabilized on amine-modified zeolite: antibacterial and catalytic activities for environmental pollution remediation in aqueous medium. Sep. Purif. Technol. **239**, 116542 (2020)
17. V.S. Gurina, V.P. Petranovskii, M.-A. Hernandez, N.E. Bogdanchikova, A.A. Alexeenko, Silver and copper clusters and small particles stabilized within nanoporous silicate-based materials. Mater. Sci. Eng., A **391**, 71–76 (2005)
18. Hu. Xiaosong, J. Bai, H. Hong, C. Li, Supercritical carbon dioxide anchored highly dispersed silver nanoparticles on 4A-zeolite and selective oxidation of styrene performance. CrystEngComm **18**, 2469–2476 (2016)
19. A. GhavamiNejad, A. Kalantarifard, G.S. Yang, C.S. Kim, In-situ immobilization of silver nanoparticles on ZSM-5 type zeolite by catechol redox chemistry, a green catalyst For A^3-coupling reaction. Microporous Mesoporous Mater. **225**, 296–302 (2016)
20. J. Milenkovic, J. Hrenovic, D. Matijasevic, M. Niksic, N. Rajic, Bactericidal activity of Cu-, Zn-, and Ag-containing zeolites toward Escherichia coli isolates. Environ Sci Pollut Res **24**, 20273–20281 (2017)
21. M.I. Panayotova, N.N. Mintcheva, O.T. Gemishev, G.T. Tyuliev, G.D. Gicheva, L.P. Djerahov, Preparation and antimicrobial properties of silver nanoparticles supported by natural zeolite clinoptilolite. Bul. Chem. Commun. **50**, 211–218 (2018)
22. A. Amirjani, D.H. Fatmehsari, Colorimetric detection of ammonia using smartphones based on localized surface plasmon resonance of silver nanoparticles. Talanta **176**, 242–246 (2018)
23. NG Mlalila, HS Swai, A Hilonga, DM Kadam, Antimicrobial dependence of silver nanoparticles on surface plasmon resonance bands against *Escherichia coli,* Nanotechnol. Sci. Appl. 10: 1–9, (2017)
24. J.R. Koduru, S.K. Kailasa, J.R. Bhamore, K.-H. Kim, T. Dutta, K. Vellingiri, Adv. Colloid Interface Sci. **256**, 326–339 (2018)
25. R. Rafique, S.K. Kailasa, T.J. Park, TrAC Trends Anal. Chem. **120**, 115646 (2019)
26. M. Ashrafizadeh, R. Mohammadinejad, S.K. Kailasa, Z. Ahmadi, E.G. Afshar, A. Pardakhty, Adv. Colloid Interface Sci. **278**, 102123 (2020)
27. G.E. Machado, A.M. Pereyra, V.G. Rosato, M.S. Moreno, E.I. Basaldella, Improving the biocidal activity of outdoor coating formulations by using zeolite-supported silver nanoparticles. Mater. Sci. Eng., C **98**, 789–799 (2019)
28. M. Li, L. Gao, C. Schlaich, J. Zhang, I.S. Donskyi, Yu. Guozhi, W. Li, Tu. Zhaoxu, J. Rolff, T. Schwerdtle, R. Haag, N. Ma, Construction of functional coatings with durable and broad-spectrum antibacterial potential based on mussel-inspired

dendritic polyglycerol and in situ-formed copper nanoparticles. ACS Appl. Mater. Interfaces **40**, 35411–35418 (2017)
29. D. Jiraroj, S. Tungasmita, D.N. Tungasmita, Silver ions and silver nanoparticles in zeolite A composites for antibacterial activity. Powder Technol. **264**, 418–422 (2014)
30. L. Mpenyana-Monyatsi, N.H. Mthombeni, M.S. Onyango, M.N.B. Momba, Cost-effective filter materials coated with silver nanoparticles for the removal of pathogenic bacteria in groundwater. Int. J. Environ. Res. Public Health **9**, 244–271 (2012)
31. B. Galeano, E. Korff, WL Nicholson, Inactivation of Vegetative Cells, but Not Spores, of Bacillus anthracis, B. cereus, and B. subtilis on Stainless Steel Surfaces Coated with an Antimicrobial Silver- and Zinc-Containing Zeolite Formulation, applied and Environmental Microbiology, 4329–4331, (2003)
32. J.F. Román-Zamorano, M. Flores-Acosta, H. Arizpe-Chávez, F.F. Castillón-Barraza, M.H. Farías, R. Ramírez-Bon, Structure and properties of lead and lead sulfide nanoparticles in natural zeolite. J. Mater. Sci. **44**, 4781–4788 (2009)
33. N.S. Flores-Lopez, Nanopartículas de Ag en Zeolitas A4 y Chabazita. Professional thesis. Centro de Investigación en Materiales Avanzados, S. C. 13, 34
34. N.S. Flores-López, J. Castro-Rosas, R. Ramírez-Bon, A. Mendoza-Córdova, E. Larios-Rodríguez, M. Flores-Acosta, Synthesis and properties of crystalline silver nanoparticles supported in natural zeolite chabazite. J. Mol. Struct. **1028**, 110–111 (2012)
35. E. Torres, Síntesis de Nanopartículas de Plata en Chabazita, para la Elaboración de Recubrimientos Bactericidas. Tesis profesional. Universidad de Sonora. 15–46, (2016)
36. M. John, S. William, B.K. Sobol Peter, Handbook of X-ray Photoelectron Spectroscopy. Edited by Jill Chastain. Minnesota, E.U.A. Perkin-Elmer Corporation. 120–121, (1993)
37. M.D. Martínez de Yuso García, Aplicaciones de la Espectroscopía Fotoelectrónica de Rayos X en la Caracterización de Materiales Funcionales. Facultad de Ciencias. Universidad de Málaga. 7–8, (2015)
38. Á.B. Sifontes, L. Melo, C. Maza, J.J. Mendes, M. Mediavilla, Preparación de Nanopartículas de Plata en Ausencia de Polimeros Estabilizantes. Química Nova **33**(6), 1266–1269 (2010)
39. G.A.C.M. Spierings, Optical absorption of Ag+ ions in 11(Na, Ag)2O · 11B2O3 · 78SiO2 glass. J. Non-Cryst. Solids **94**, 407–411 (1987)
40. G. Barcaro, M. Broyer, N. Durante, A. Fortunelli, M. Stener, Alloying effects on the optical properties of Ag-Au nanoclusters from TDDFT calculations. J. Phys. Chem. C **115**, 24085–24091 (2011)
41. K. Natarajan, S. Selvaraj, V.R. Murty, Microbial production of silver nanoparticles. Digest J Nanomater Biostruct **5**, 135–140 (2010)
42. H. Lee, G. Ro, J.M. Kim, Y. Kim, Discrete-dipole approximation for the optical properties with morphological changes of silver nanoprism and nanosphere via galvanic reaction. Mater. Lett. **209**, 138–141 (2017)
43. D.H. Kim, J.C. Park, G.E. Jeon, C.S. Kim, J.H. Seo, Effect of the size and shape of silver nanoparticles on bacterial growth and metabolism by monitoring optical density and fluorescence intensity. Biotechnol. Bioprocess Eng. **22**, 210–217 (2017)
44. A.L. González, C. Noguez, Influence of morphology on the optical properties of metal nanoparticles. J Comput Theoretical Nanosci. **4**, 231–238 (2007)
45. L.B. Gulina, G. Korotcenkov, B.K. Cho, S.H. Han, V.P. Tolstoy, Ag nanoclusters synthesized by successive ionic layer deposition-method and their characterization. J Mater Sci **46**, 4555–4561 (2011)
46. F. Collins, A. Rozhkovskaya, J.G. Outram, G.J. Millar, A critical review of waste resources, synthesis, and applications for Zeolite LTA. Microporous Mesoporous Mater. **291**, 109667 (2020)
47. J. Singh, R.L. White, A variable temperature infrared spectroscopy study of NaA zeolite dehydration. Vib. Spectrosc. **94**, 37–42 (2018)
48. M. Król, W. Mozgawa, W. Jastrzebski, K. Barczyk, Application of IR spectra in the studies of zeolites from D4R and D6R structural groups. Microporous Mesoporous Mater. **156**, 181–188 (2012)
49. N.N. Safie, A.Z. Yaser, N. Hilal, Ammonium ion removal using activated zeolite and chitosan. Asia-Pac J Chem Eng. **15**, e2448 (2020)
50. M.R. Abukhadra, S.M. Ibrahima, S.M. Yakout, M.E. El-Zaidy, A.A. Abdeltawab, Synthesis of Na+ trapped bentonite/zeolite-P composite as a novel catalyst for effective production of biodiesel from palm oil; effect of ultrasonic irradiation and mechanism. Energy Conversion Manage. **196**, 739–750 (2019)
51. M. Nabiollah, N. Rikhtegar, H.A. Panahi, A. Farideh, B.K. Shahraki, Porosity, characterization and structural properties of natural zeolite—clinoptilolite—as a sorbent. Environ. Protect. Eng. **39**, 139–152 (2013)
52. A.D. Montes-Luna, N.C. Fuentes-López, Y.A. Perera-Mercado, O. Pérez-Camacho, G. Castruita-de León, S.P. García-Rodríguez, M. García-Zamora, Caracterización de Clinoptilolita Natural y Modificada con Ca2+ por Distintos Métodos Físico-Químicos para su Posible Aplicación en Procesos de Separación de Gases. Sociedad Mexicana Ciencia Tecnología Superficies Materiales. **28**, 5–11 (2015)
53. T.M. Piqué, A. Vázquez, Uso de Espectroscopía Infrarroja con Transformada de Fourier (FTIR) en el Estudio de la Hidratación del Cemento. Concreto Y Cemento. Investigación Y Desarrollo **3**, 62–71 (2012)
54. D. Novgorodova, A. Gorshkov, A. Mokhov, Standard X-ray diffraction powder patterns. Zap. Vses. Mineral. O-va. **108**, 552–554 (1979)
55. M.L. Lind, A.K. Ghosh, A. Jawor, X. Huang, W. Hou, Y. Yang, E.M.V. Hoek, Influence of zeolite crystal size on zeolite-polyamide thin film nanocomposite membranes. Langmuir **25**, 10139–10145 (2009)
56. E. Kolobova, A. Pestryakov, G. Mamontov, Y. Kotolevich, N. Ogdanchikova, M. Farias, A. Vosmerikov, L. Vosmerikova, V. Cortes Corberan, Low-temperature CO oxidation on Ag/ZSM-5 catalysts: Influence of Si/Al ratio and redox pretreatments on formation of silver active sites. Fuel **188**, 121–131 (2017)
57. A. Nagy, A. Harrison, S. Sabbani, R.S. Munson Jr., P.K. Dutta, W.J. Waldman, Silver nanoparticles embedded in zeolite membranes: release of silver ions and mechanism of antibacterial action. Int. J. Nanomed. **6**, 1833–1852 (2011)
58. H. Khodabandehloo, H. Zahednasab, A.A. Hafez, Nanocarriers usage for drug delivery in cancer therapy, Iran. J. Cancer Prev. **9**, e3966 (2016)
59. D. Ho, X. Sun, S. Sun, Monodisperse magnetic nanoparticles for theranostic applications. Acc. Chem. Res. **44**, 875–882 (2011)
60. T. Miyanaga, H. Hoshino, H. Endo, Local structure of silver clusters in the channels of zeolite 4A. J. Synchrotron Rad. **8**, 557–559 (2001)
61. Y. Chai, W. Shang, W. Li, Wu. Guangjun, W. Dai, N. Guan, L. Li, Noble metal particles confined in zeolites: synthesis, characterization, and applications. Adv. Sci. **6**, 1900299 (2019)
62. M.J. Sánchez, J.E. Mauricio, A.R. Paredes, P. Gamero, D. Cortés, Antimicrobial properties of ZSM-5 type zeolite functionalized with silver. Mater. Lett. **191**, 65–68 (2017)
63. L. Zhu, S. Ye, A. Asghar, S.-H. Bang, Oh. Won-Chun, Additional effect of zeolite based on bactericidal activated carbon spheres

with enhanced adsorption effect and higher ignition temperature. J. Korean Ceram. Soc. **53**, 68–74 (2016)
64. M. Vanaja, G. Annadurai, Coleus aromaticus leaf extract mediated synthesis of silver nanoparticles and its bactericidal Activity. Appl Nanosci **3**, 217–223 (2013)
65. A. Ávalos, A.I. Haza, D. Mateo, P. Morales, Nanopartículas de plata: aplicaciones y riesgos tóxicos para la salud humana y el medio ambiente. Rev Complutense Ciencias Veterinarias. **7**, 1–23 (2013)
66. Y.H. Tan, Y. Chen, W.H.W. Chu, L.-T. Sham, Y.-H. Gan, Cell envelope defects of different capsule-null mutants in K1 hypervirulent Klebsiella pneumoniae can affect bacterial pathogenesis. Mol. Microbiol. **113**, 889–905 (2020)